Ain Shams Engineering Journal 16 (2025) 103489

Contents lists available at ScienceDirect

Ain Shams Engineering Journal

journal homepage: www.sciencedirect.com

Differentiator circuits with scalable and electronically adjustable time constant and their application in phase shift evaluation

Roman Sotner [a,b,*], Ladislav Polak [a], Jiri Petrzela [a,b], Dmitrii Semenov [a], Lukas Langhammer [a,b], Winai Jaikla [c]

[a] Department of Radio Electronics, Faculty of Electrical Engineering and Communications, Brno University of Technology, Technicka 12, 616 00 Brno, Czech Republic
[b] Department of Electrical Engineering, Faculty of Military Technology, University of Defence, Sumavska 4, Brno 602 00, Czech Republic
[c] Faculty of Industrial Education and Technology, King Mongkut's Institute of Technology Ladkrabang, Bangkok 10520, Thailand

ARTICLE INFO

Keywords:
Differentiator
Electronic adjustment
Operational amplifier
Scaling
Phase shift measurement
Time constant
Variable gain amplifier

ABSTRACT

Two novel scalable and electronically adjustable differentiator designs are presented in this paper. These designs are based on special variable gain amplifiers extending well-known concept of standard single operational amplifier-based differentiators. The key novelty lies in their scalability, which allows for an enhanced time constant value by adjusting the ratio of resistors. Simultaneously, the special form of gain control using a DC voltage offers wide electronic tunability. The solution performs high input and low output impedance, both independent of frequency. Experimental testing demonstrated time constant adjustments in two configurations: from 64 ns to 4.5 μs (a ratio of maximal and minimal value 70) and from 8.7 μs to 183 μs (a ratio of 21). As an application example, the proposed differentiator is utilized in the design of a readout system for an absolute phase shift difference to pulse width ratio converter, suitable for monitoring a very slow phenomenon such biosignals.

1. Introduction

Modern analog chip designs prevent the use of large value capacitors due to their impracticality for integration, as they require a significant amount of chip area [1]. This issue is not limited to integrated circuits but also affects discrete systems operating at very slow, low-frequency signals (from sub-Hz to tens of Hz). In such cases, large value capacitors occupy a significant space on printed circuit boards (PCBs), especially when using small surface mount devices (SMDs). However, very high capacitance values (in the range of μF or hundreds of nF) are often required at many places, particularly for decoupling applications [2,3].

Several methods have been proposed [4–14] to create so called active solutions that enhance capacitance values (or general ideal impedance response [5,8,9]) through active circuit gain. These methods primarily focus on capacitance multiplication, where the effective capacitance is increased by a multiplication constant (or scaling factor) [4,6,7,10,11–14]. In some cases, electronic adjustment is not necessary, as fixed scalability can be achieved by passive elements [6,10]. However, many designs allow both capacitance boosting/scaling and electronic adjustment [4,5,7–9,11–14]. Next, many capacitance multiplier circuits achieve a boosted value for grounded capacitance or inductance [5,8–10,11,12,13]. However, some topologies – or their internal solutions – become significantly more complex when implementing floating elements [4,7,12,14]. It is important to note that floating elements are essential in operational amplifier-based solutions for various building blocks and applications. A comprehensive review of impedance and capacitance multipliers was recently published by Senani et al. [15], summarizing over 250 different solutions. However, a detailed discussion of these designs is beyond the scope of this work. Recent research (from 2022 to 2024) highlights the growing interest capacitance multiplication among researchers worldwide. However, most studies have focus solely on linear filtering applications [16,17]. This work, on the other hand, demonstrates several additional beneficial implementations.

The operational amplifier-based lossless differentiator is a typical example of a building block where a floating capacitor is used [16,17]. Additionally, the standard solution of differentiator with an operational amplifier (opamp) has a frequency dependent input impedance, which is

* Corresponding author.
E-mail addresses: sotner@vut.cz (R. Sotner), polakl@vut.cz (L. Polak), petrzela@vut.cz (J. Petrzela), 240689@vut.cz (D. Semenov), langhammer@vut.cz (L. Langhammer), winai.ja@kmitl.ac.th (W. Jaikla).

https://doi.org/10.1016/j.asej.2025.103489
Received 11 February 2025; Received in revised form 23 April 2025; Accepted 12 May 2025
Available online 31 May 2025

Table 1
Comparison of typical and similar lossless differentiator solutions with the proposed circuit designs.

Reference	Total no. of active elements	No. of active elements responsible for capacity electronic adjustment	No. of passive elements (floating/ grounded)	Impedance character (input/ output)	Frequency independent input impedance	Time constant defined by passive and active parameters simultaneously	Scaling of time constant	Method of scaling	Electronic adjustment of time constant	Input/output impedance independent on electronic adjustment of time constant	Method of time constant electronic adjustment (driving)	Linear adjustment	Operation mode
[16,17,19] *	1	0	2/0	Low/Low	No	No	No	–	No	–	–	–	voltage
[20]	2–3	0	2–3/0–1	Low/High	No	No	No	–	No	–	–	–	current
[21]	2	1	0–1/1–2	High/Low	Yes	Yes	No	–	Yes	Yes	voltage	Yes	voltage
[22]	1	0	1/1	Low/High	No	No	No	–	No	–	–	–	current
[23]	2	2	1/1	Low/High	Yes	Yes	No	–	Yes	N/A	current	Yes	current
[24]	1	1	2/0	High/Low	Yes	Yes	No	–	Yes	Yes	voltage	Yes	voltage
[25]	1	0	1/1	Low/Low	No	No	No	–	No	–	–	–	voltage
[26]**	1	0	2/0	Low/Low	No	Yes	No	–	Yes	Yes	voltage	N/A	voltage
[27,28] ***	2	1	0/0	Low/High	N/A	Yes	N/A	N/A	Yes	N/A	current	N/A	current
[29]	2	0	1/3	High/Low	Yes	No	Yes	ratio of resistors	No	–	–	–	voltage
[30,31]	2	2	0/1	Low/High	N/A	Yes	No	–	Yes	N/A	current	No	current
[32]	1	1	1/0	Low/Low	No	Yes	No	–	Yes	N/A	current	N/A	current
[33]	2	1	0/1	Low/High	N/A	Yes	No	–	Yes	N/A	current	No	current
[34]	1	0	2/0	Low/Low	No	No	No	–	No	–	–	–	voltage
This work (Fig. 2)	2	1	4/0	High/Low	Yes	Yes	Yes	ratio of resistors	Yes	Yes	voltage	Yes	voltage
This work (Fig. 4)	2	1	3/1	High/Low	Yes	Yes	Yes	ratio of resistors	Yes	Yes	voltage	Yes	voltage

*a well-known standard solution using operational amplifier (opamp), capacitor and resistor.
**replacement of a feedback resistor by a variable MOS-based resistor.
***use of real parasitic features of opamp (single-pole model), many key features for comparison purposes are not tested and shown (only basic theoretical analysis is available), two electronically adjustable parameters are available for time constant adjustment.
N/A – information not available/explained or visible from available formulas and results.

a significant issue when the excitation signal is not properly buffered (i.e., lacks impedance separation). However, some two-port solutions for lossless differentiator can be implemented without relying on the complex floating capacitor multiplier solutions discussed earlier. The fundamental principle behind time constant scaling and adjustment is the use of Miller effect [13,14,18]. This phenomenon multiplies the capacitance in the time constant by a certain factor, which can be determined by the gain of the active circuit. This factor is defined by a parameter of an active device or parameter based on external elements outside of the active device. This multiplication factor (a constant) may be fixed (called the scaling factor), electronically adjustable, or both simultaneously. These aspects are analyzed independently in the following sections.

Table 1 presents a comparison of various differentiator solutions, highlighting key properties such as ease of implementation, potential conflicts in further circuit integration, performance, and the availability of fixed scalability and electronic adjustability of the time constant. The analysis of these solutions, summarized in Table 1, leads to several important observations:

a) Some existing solutions, including recent ones, do not focus on the electronic adjustment of the time constant of the differentiator [19,20,22,25,29,34].
b) The scalability (i.e., boosting) of the time constant using a fixed multiplication factor is possible in limited cases [29].
c) Electronic time constant adjustment has been used several times [21,23,24,26–28,30–33], though information about the dependency, trend and range adjustment is rarely provided [21,23,24].
d) The input and output impedance characteristics are not optimal for cascading in several cases [19,25,26,34].
e) In some designs, the impact of the electronic adjustment process on the input or output impedance of the differentiator remains uncertain [23,27,28,30–33].
f) Many solutions operate in the current mode [20,22,23,27,28,30–33].

Only solutions that allow fixed scaling require two additional passive elements (resistors) to set the scale [29]. However, these elements are useful for achieving a fixed scaling factor, enabling a significant increase (or decrease) in the time constant value compared to the original. In the simplest case, this scaling is achieved by multiplying the mathematical product of the original capacitor value by a parameter such as resistor [19], transconductance [30] or the resistance of a current input terminal [33] in the circuit. All electronically adjustable solutions have similar complexity, requiring at most two active devices. The most comparable designs to our newly presented concepts can be found in [21] and [24]. Both solutions utilize commercially available devices, making them easy to access and implement.

However, neither of these designs incorporates additional scaling beyond electronic adjustment. It seems that the simultaneous use of a fixed scalability factor and electronic adjustment in differentiators has not been previously explored. Furthermore, most of the aforementioned solutions do not provide detailed information on key qualitative parameters such as tunability and adjustability ranges or required driving voltage ranges.

The limitations of prior solutions motivated our research, leading to the following objectives, which we aim to fulfill simultaneously:

a) High input impedance.
b) Low input impedance.
c) Frequency-independent input and output impedance in ideal topologies.
d) Input and output impedances independent on the electronic adjustment process.
e) Configurable scalability (fixed multiplication constant) of the time constant.
f) Linear and continuous electronic adjustability of the time constant.
g) A maximum of two commercially available active devices.
h) A maximum of two additional circuit elements for fixed multiplication constant scaling (with a preference for scaling via element ratios).

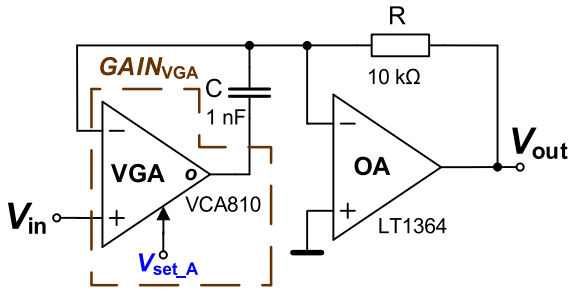

Fig. 1. The adjustable differentiator using the simplest VGA (VCA810) – a fundamental concept.

All verifications of the proposed concepts are based on experiments using commercially available off-the-shelf components. This approach is sufficient to confirm both the functionality and feasibility of the discrete design. However, current trends in electronics favor the integration of complete analog systems and front-end components onto a single chip, which significantly reduces circuit size. Despite this advantage, integrated design is very expensive at all stages – from the design and to fabrication – and is more suitable for mass production of final products rather than for initial verification of ideas, principles or concepts. Therefore, we chose to use discrete components to demonstrate the feasibility and potential applications of our concepts. The active devices used can be integrated onto a chip with some limitations (such as gain range, linearity, dynamic range, frequency response, and DC accuracy). Nevertheless, the circuit ideas and principles presented in this work are reproducible and practically realizable.

The rest of this paper is organized as follows. Section 2 introduces the principle of time constant adjustment using a variable gain amplifier (VGA) and defines the two proposed solutions, including the features of selected devices. Section 3 presents an experimental analysis of both differentiator designs, as well as the most significant parasitic effects generated by real circuitry. The final part of Section 3 demonstrates an application example in the form of a readout for absolute phase shift difference evaluation. Finally, Section 4 concludes this paper.

2. Adjustable differentiator solutions

Modern VGAs are available in various forms of devices, each offering significant advantages in terms of adjustability range, terminal characteristics, and frequency response. For this study, we selected only up-to-date and commercially available devices that provide notable benefits. The opamps used in our design are the LT1364 [35] and OPA2652 [36]. The most important features of these devices are summarized in Table A1 and Table A2 in the Appendix **A**.

Fig. 1 illustrates a differentiator based on a VGA, specifically using the VCA810 [37] as an example. This solution represents the fundamental theoretical concept behind the proposed design. The VGA in this setup operates on the basic ideal principle $v_o = (v_+ - v_-)\cdot A$), where the adjustable gain is defined as $A = 10^{2(|\mathrm{Vset\_A}| - 1)}$. Hereby, the ideal transfer response

$$K_{diff}(s) = -sCR\cdot GAIN_{VGA} = -sCR\cdot A = -sCR\cdot 10^{2(|V_{set\_A}|-1)} \quad (1)$$

indicates an exponential dependence of the time constant on the V_{set_A} voltage. The time constant is given by $\tau_{diff} = C\cdot R\cdot 10^{2(|\mathrm{Vset\_A}| - 1)}$. The gain A can be adjusted from 0.01 to 100. However, such a wide gain range has certain limitations when very low gain values lead to noise issues or very

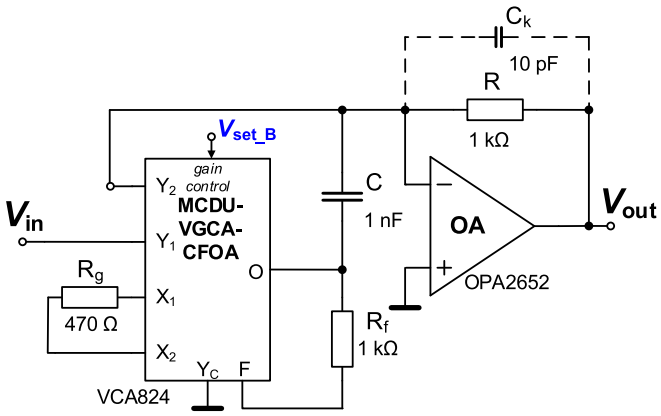

Fig. 2. The adjustable differentiator using the special VGA VCA824.

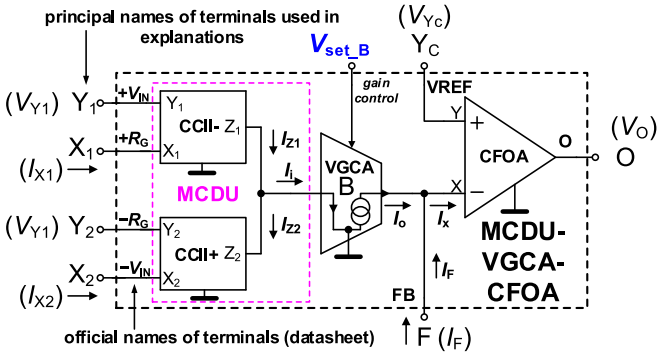

Fig. 3. Internal concept of MCDU-VGCA-CFOA (VCA824) [43].

high gain values may cause saturation due to small DC voltage offsets. Nevertheless, the topology shown in Fig. 1 presents the fundamental concept of an adjustable differentiator. The design employs a standard opamp with a feedback resistor and the simplest VGA for gain adjustment. The fixed scaling factor is not implemented in this solution. It is important to mention that all differentiators in this study have an inverting behavior due to the origin of topology using the inverting stage of opamp.

The solution presented in Fig. 2 enhances the versatility of the differentiator by introducing time constant scalability through additional parameters, achieved by implementing the VCA824 VGA device [38]. This device has internal topology depicted in Fig. 3. The name of the device reflects its underlying operational principles, combining multiple functional units: a modified current differencing unit (MCDU) [39–42], a variable gain current amplifier (VGCA) [39–41], and a current feedback operational amplifier (CFOA) [39–41], collectively referred to as MCDU-VGCA-CFOA [43]. The detailed principle is explained in Appendix **B**. Then the adjustable voltage in Fig. 2 is defined as $A = B{\cdot}2R_f/R_g$. Due to the high-frequency nature of the VCA824, the high-speed, high-frequency OPA2652 opamp is used in this configuration (both devices have similar performance).

The ideal transfer function of the differentiator shown in Fig. 2 is given by:

$$K_{diff}(s) = -sCR{\cdot}GAIN_{VGA} = -sCR{\cdot}\left(\frac{2{\cdot}B{\cdot}R_f}{R_g}\right) \cong -sCR{\cdot}\left[\frac{(V_{set\_B}+1){\cdot}R_f}{R_g}\right] \quad (2)$$

The corresponding time constant $\tau_{diff} = C{\cdot}R{\cdot}(V_{set\_B}+1){\cdot}R_f/R_g$ shows a linear dependency on the voltage V_{set_B}. Compared to (1) and the previous solution, this approach offers greater flexibility in adjusting the time constant due to the additional degree of freedom introduced by the ratio of R_f and R_g.

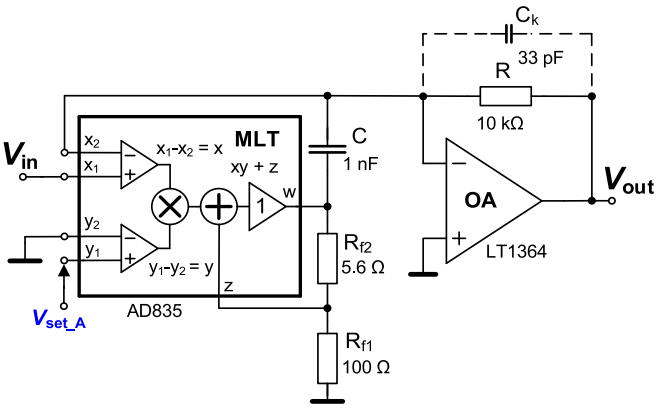

Fig. 4. The adjustable differentiator using the special VGA AD835 device.

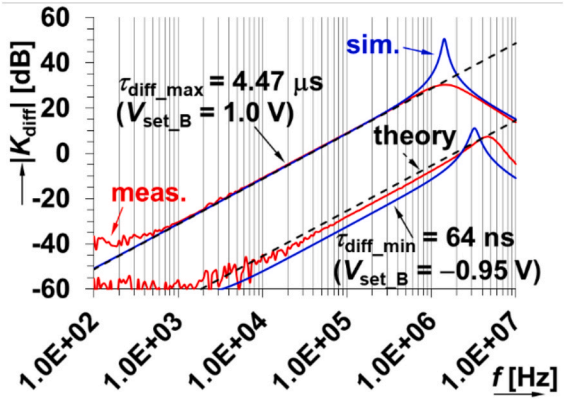

Fig. 5. Experimental verification of the adjustable differentiator from Fig. 2 (magnitude responses).

Fig. 4 shows an alternative solution using the AD835 voltage-mode multiplier [44] as the VGA. The ideal operation of the multiplier has the following form: $v_w = (v_{x1} - v_{x2}){\cdot}(v_{y1} - v_{y2}){\cdot}k + v_z$, where $k \cong 1$ is the intrinsic constant of the multiplier. All inputs, including the auxiliary terminal z, have high-impedance voltage character, while the output terminal w has a low-impedance character. The feedback resistors R_{f1}, R_{f2} enable the formation of the VGA gain, defined as: $A \cong V_{set\_A} \cdot (1 + R_{f1}/R_{f2})$. Accordingly, the ideal transfer function of the differentiator in Fig. 4 is:

$$K_{diff}(s) = -sCR{\cdot}GAIN_{VGA} = -sCR{\cdot}A \cong -sCR{\cdot}V_{set\_A}{\cdot}\left(1+\frac{R_{f1}}{R_{f2}}\right) \quad (3)$$

The time constant scalability is determined by the ratio of R_{f1} and R_{f2}, while V_{set_A} allows for continuous adjustment of the time constant $\tau_{diff} = C{\cdot}R{\cdot}V_{set\_A} \cdot (1 + R_{f1}/R_{f2})$.

3. The verification

3.1. Analysis of differentiators

This section presents the analysis of the features of differentiators from both solutions shown in Fig. 2 and Fig. 4. The evaluation focuses on the behavior in the frequency domain. Measurements were made using a Keysight DSO-X 3024 T oscilloscope. The input signal frequency was varied from 100 Hz to 10 MHz, with input voltage amplitudes ranging from 20 mV to 100 mV. The circuits were powered by a ± 5 V supply voltage.

For the first solution in Fig. 2 (VCA824 and OPA2652), the initial time constant was determined by the following passive element values:

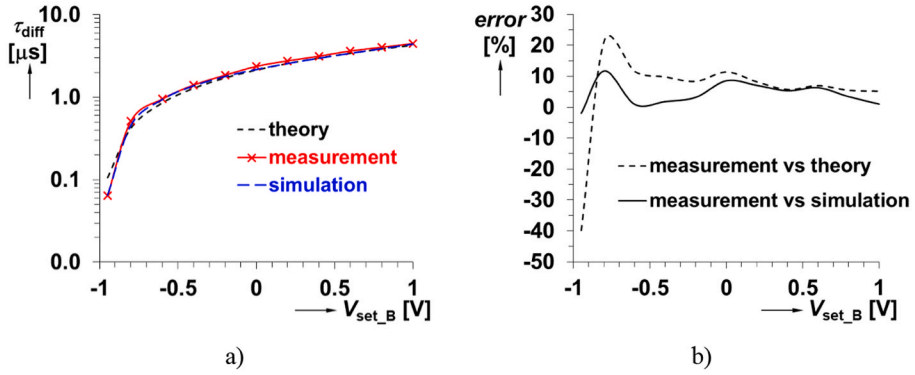

Fig. 6. The adjustability of the time constant of the solution in Fig. 2: a) the dependence of the time constant on the driving voltage, b) evaluation of the error.

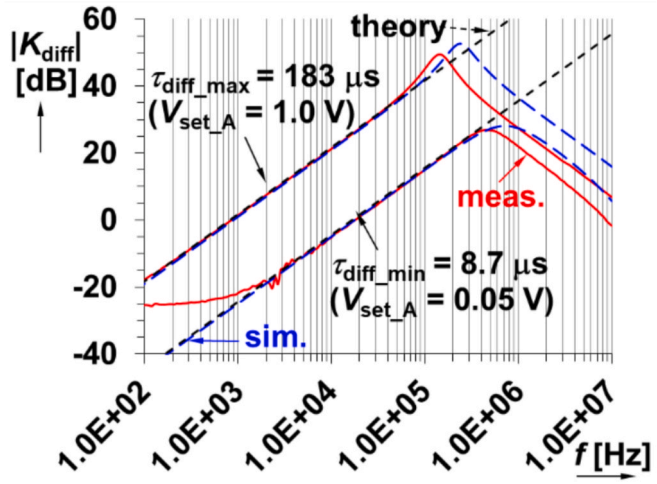

Fig. 7. The experimental verification of adjustable differentiator from Fig. 4 (magnitude responses).

$R = 1$ kΩ, $C = 1$ nF, $R_g = 470$ Ω and $R_f = 1$ kΩ (both auxiliary elements), and compensation capacitor $C_k = 10$ pF. Under these conditions, the expected (ideal) time constant at $V_{set\_B} = 0$ V is $t_{diff} = 2.13$ μs. For comparison, a standard opamp-based lossless differentiator, using only R and C, would yield a fixed time constant of 1 μs for the same component values. The ideal range of time constant variability is expected to span from 106 ns to 4.26 μs (for $V_{set\_B} = -0.95$ V and 1 V). The dependence is linear based on the definition of the adjustable gain of the VCA824. The simulated range is from 65 ns to 4.43 μs and the measured range was obtained between 64 ns and 4.47 μs (the measured ratio of τ_{diff_max} and τ_{diff_min} is 70).

Fig. 5 shows the comparison of the ideal, simulated, and measured results for the minimum and maximum time constant at low frequencies and high attenuation values. The measured differentiator indicates reliable differentiation behavior with the frequency range of 2 kHz to 200 kHz (spanning of two frequency decades) for the selected RC values (time constant). Fig. 6 captures the time constant adjustability range and the errors between theoretical, simulated, and measured results.

The error between theory and measured values is approximately 10 % for most of the V_{set_B} range. For very low values of V_{set_B}, it exceeds 20 %. However, the discrepancy between simulation and measurement remains within 11 % across the full range.

The second solution shown in Fig. 4 (AD835 and LT1364) was tested for an expected (ideal) initial time constant of $t_{diff} = 192$ μs at $V_{set\_A} = 1$ V. The parameters of circuit elements, including auxiliary resistors $R_{f1} = 100$ Ω, $R_{f2} = 5.6$ Ω and compensation capacitor $C_k = 33$ pF, allow for a theoretical time constant adjustment range from 9.6 μs to 192 μs (for V_{set_A} ranging from 0.05 V to 1 V). For comparison, a standard opamp-based lossless differentiator (using only R and C) has a fixed time constant of 10 μs, assuming $R = 10$ kΩ and $C = 1$ nF, which are the same values used in Fig. 4. The simulation results range from 9 μs to 179 μs while the measured results range from 8.7 μs to 183 μs. Fig. 7 presents an example of the minimum and maximum achievable time constant values. The operational frequency range is estimated to be 2 kHz to 80 kHz, given the selected parameter settings. The differences observed in linear response plots (see Fig. 8) indicate a very low error of up to 9 % and 3 % for measurement vs theory and measurement vs simulation, respectively. These results indicate higher accuracy than the solution in Fig. 2, but the time constant adjustment range is narrower compared to the previous case (the measured ratio of τ_{diff_max} and τ_{diff_min} is 21). For this circuit solutions, the differentiation performance in the time domain was evaluated. For this purpose, typical examples of waveforms were selected. Fig. 9 illustrates four representative waveforms at frequencies within the differentiation range: sine wave, square wave, triangular

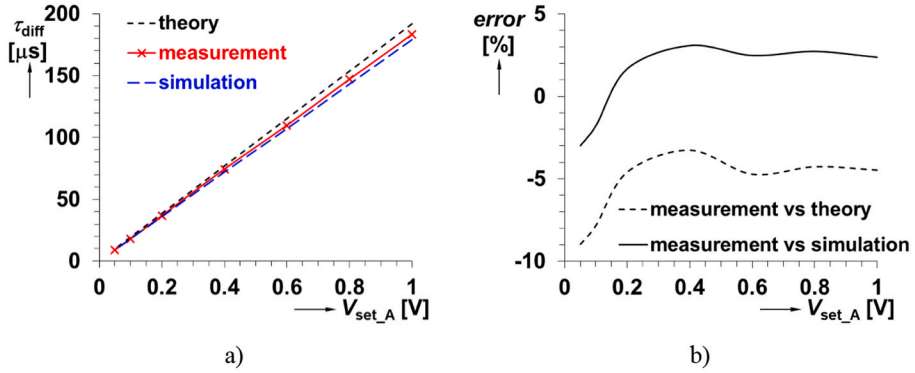

Fig. 8. The adjustability of time constant of solution in Fig. 4: a) the dependence of time constant on driving voltage, b) error evaluation.

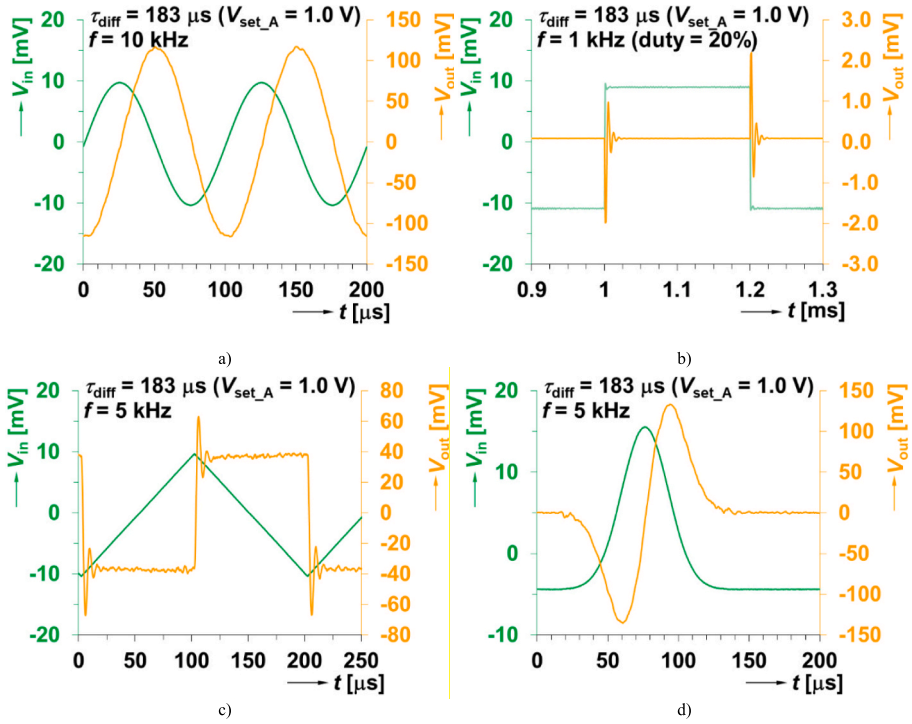

Fig. 9. The example of measured differentiation of selected waveforms: a) sine wave, b) square wave, c) triangular wave, d) Gaussian impulse.

Table 2
Comparison of solutions introduced in Fig. 2 and Fig. 4.

parameter	Fig. 2	Fig. 4
DC voltage adjustability range	−0.95 → 1 V	0.05 → 1 V
Single polarity DC voltage range	No	Yes
Time constant variability	64 ns → 4.47 µs	8.7 µs → 183 µs
Time constant ratio range $\tau_{diff\_max}/\tau_{diff\_min}$	70	21
Fixed time constant scale factor based on auxiliary resistors	2	19
Electronic adjustability extension	Yes	No
Number of passive elements	4	4
Number of active elements	2	2
Observed approximate differentiation range	50–60 dB	40–50 dB
Observed frequency range of operation (precise differentiation)	2 kHz → 200 kHz	2 kHz → 80 kHz
Stability and self-oscillation issues possibility	high	medium
Approximate maximal temperature instability of value (−20 → +40 °C)	±15 %	N/A (not modelled)
Approximate maximal supply voltage instability of value (±4 → ±6 V)	±5%	N/A

wave, and Gaussian impulse.

Table 2 compares the most significant performance aspects of both topologies introduced in Fig. 2 and Fig. 4. The time constant values and their adjustment ranges depend on the selected parameter values, meaning these values are not strictly final. The most important practical difference between both solutions is the extended adjustability range of the VCA824 (see Fig. 2). This is evident in the time constant ratio, which is 70 (see Fig. 2) compared to 21 (see Fig. 4). The overall circuit complexity of both solutions is similar. From a practical implementation perspective (as indicated in Table A1), the VCA824-baed solution (see Fig. 2) is more sensitive to proper RF compatible design than the AD835-based solution (see Fig. 4). If the device terminals are not properly terminated, or stability precautions are not applied during circuit design and printed circuit board (PCB) layout, the VCA824 circuit is more susceptible to stability issues and self-oscillations. The approximate range of monotonically increasing magnitude in the differentiation region (i.e., the difference between the maximum and minimum magnitude values in Fig. 5 and Fig. 7, where the response remains "linear" in dB scale), is 50–60 dB for both minimum and maximum time constant values in Fig. 5 and 40-50 dB in Fig. 7. This range is sufficient for many practical applications, though some limitations are introduced by the measurement equipment, particularly dynamic range and vertical resolution. Both solutions allow the time constant scaling via resistors. However, the VCA824-based differentiator offers a wider electronic adjustment range due to its special gain parameter (V_{set_B} + 1), which affects the overall time constant, particularly for very low values (negative V_{set_B}). This results in time constant ratio of 70. In contrast, the AD835-based differentiator provides a larger fixed scaling factor (19 vs. 2 in Fig. 2). In summary, while both solutions achieve comparable performance, the AD835-based solution operates over a narrower frequency range than the VCA824-based solution. However, the VCA824-based differentiator provides a greater range of time constant adjustment due to its unique gain definition but also introduces a higher risk of instability. The block diagram of the setup, the device under test (DUT), and photos of the prototypes are shown in Fig. 10.

The operational range of the device depends on the selection of time-constant-forming elements and their parameters. In other words, the operational range can be modified by appropriately choosing the values of capacitor and resistor, independently of the parameters associated with the electronically adjustable features. The examples provided in this paper serve as illustrative demonstration for proof-of-concept verification. Designers may choose different configurations of the differentiator based on their specific application requirements. Regardless of the configuration, the high-frequency limit typically falls within the range of a few MHz, primarily due to the limitations of the active components used and the real-world performance of the circuit on a PCB.

3.2. *Analysis of the most significant parasitic effects in used topology*

This section focuses on a general description of the most significant parasitic influences, using a simplified model to aid understanding. These parasitic effects increase the risk of instability and related issues.

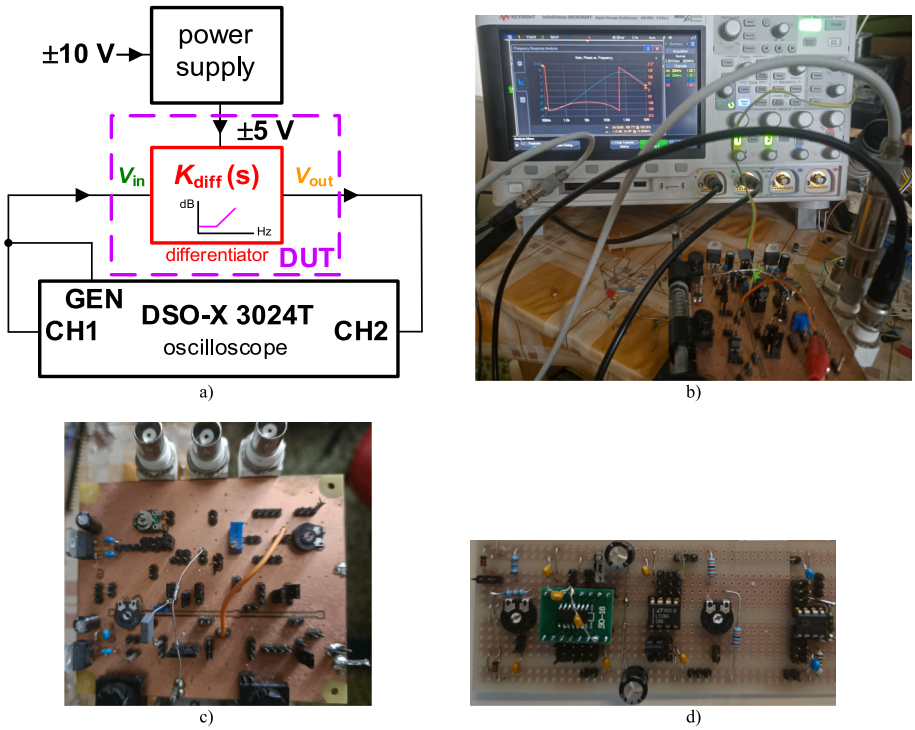

Fig. 10. The experimental setup: a) block diagram, b) photograph of the workplace including the DUT, c) module using the scheme in Fig. 2, d) module using the scheme in Fig. 4.

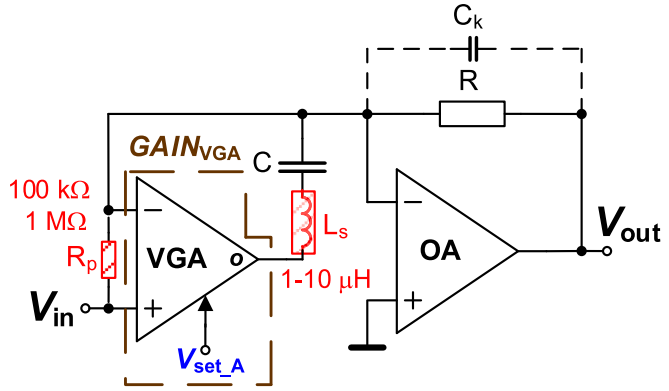

Fig. 11. The simplified model of the most significant parasitic elements in the proposed topology.

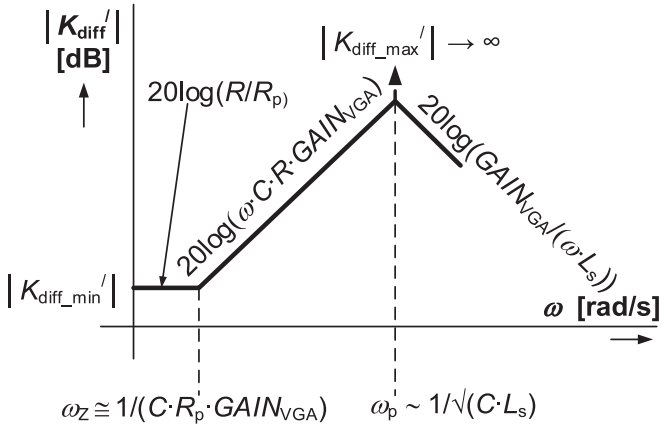

Fig. 12. Illustration of the magnitude response of the differentiator influenced by the most significant parasitic elements.

Fig. 11 shows a typical model including the most critical parasitic elements applicable to all circuits discussed in this work. One key parasitic effect is the differential input resistance R_p of the VGA, which limits the gain at low frequencies. As shown in Table 2, the R_p values are in the hundreds of kΩ, leading to an expected $|K'_{diff\_min}(\omega \to 0)|$ between −40 dB and −60 dB. It is also visible from the experimental results captured in Fig. 5. Similarly, in Fig. 7, the observed range −20 dB to −40 dB corresponds to a lower R_p value than in the first circuit (see Fig. 4). The ratio of R and R_p defines the minimum magnitude of the differentiator's frequency response. Another key issue is the resonant peak, which arises due to the serial output inductance L_s, often increased by metal wires and interconnections. The approximate value of L_s is in the low range µH (tens of µH).

Fig. 12 explains the parasitic effects described, providing useful equations for estimating their impact on the differentiator's magnitude response. These parasitic effects are particularly problematic because the gain theoretically increases to infinity at this frequency, causing a significant stability risk. Nevertheless, these issues can be easily mitigated using a compensation capacitor. Both introduced solutions include special compensation elements (capacitor C_k) used to minimize instability risks. The compensation capacitor C_k reduces the theoretically infinite gain of the differentiator at resonant frequency ($|K'_{diff\_max}(\omega_p)| = \infty$), following the approximate relation: $|K'_{diff\_max}(\omega_p)| \sim GAIN_{VGA} \cdot C/C_k$,when C_k is connected. Notably, all results presented in Fig. 5 and Fig. 7 correspond with these estimations. It is important to note that the resonant frequency ω_p is not directly dependent on the gain of the VGA. However, this dependency affects ω_p in a manner consistent with simulated and measured results. The underlying mechanism is quite complex, requiring extensive model modifications (such as a single-pole model of a real opamp) for a more precise analysis. However, such models often yield formulas that do not provide a straightforward interpretation.

Temperature variations within the range of –20 °C to + 40 °C were observed to have a maximum impact of approximately ± 15 % on the

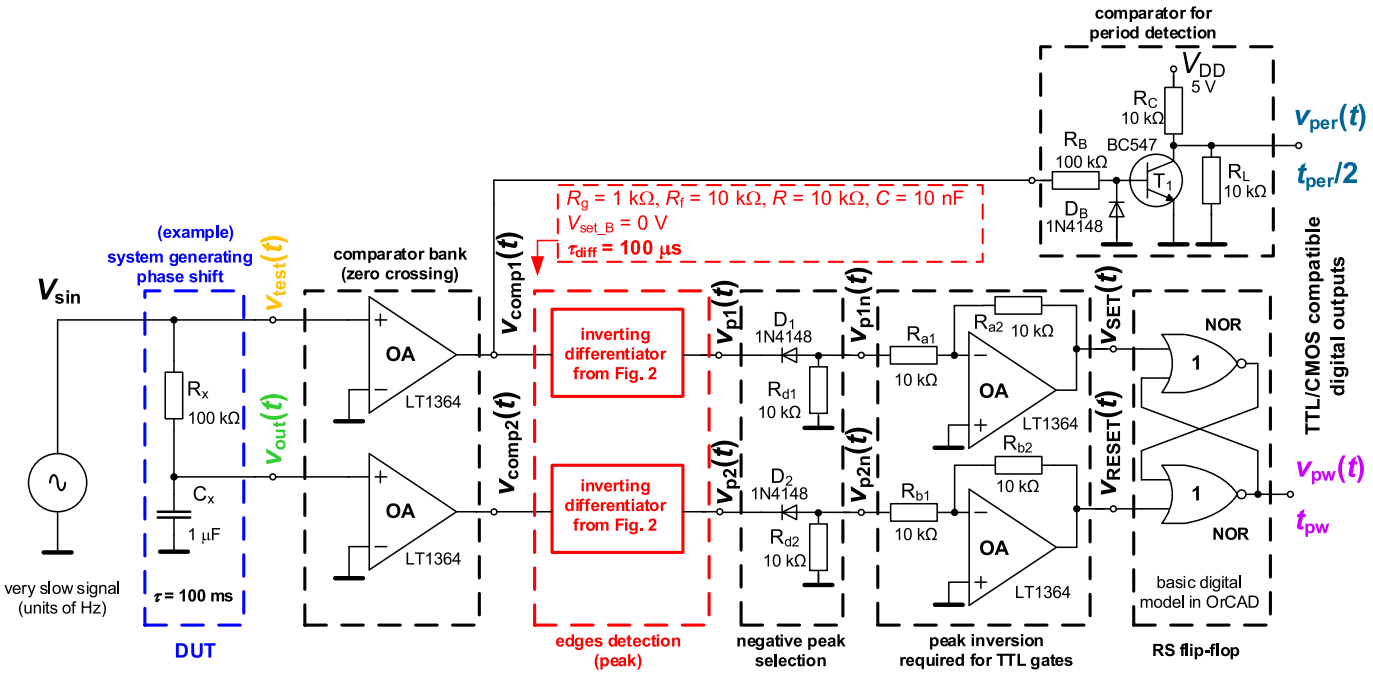

Fig. 13. Readout of the absolute value of the phase shift measurement through the digital port of the microprocessor.

capacitance value, particularly for the smallest values within the adjustable range. Similarly, supply voltage variations from ± 4 to ± 6 V introduced a maximum uncertainty of about ± 5 % at the lower end of the capacity range.

Based on a simple noise analysis simulation (noting that its accuracy may be limited due to differences between the simulated model and the real circuit, including physical realization, and uncertain noise contributions of some components), the solutions shown in Fig. 2 and Fig. 4 are comparable in terms of noise characteristics. The primary differences appear at higher frequencies due to differing parasitic resonance quality factors of both solutions.

3.3. *Application example: Readout for absolute phase difference measurement*

Integrators and differentiators are widely used in various complex industrial systems [45], particularly in instrumentation [46], measurement and sensing applications (e.g., bio-signals [47] and biomedical applications [48]). This section presents an application example focused on designing a simple readout system for measuring the absolute value of phase shift, which is calculated from the pulse width of generated impulses. The main idea is to eliminate the need for an analog-to-digital converter (ADC) in a microprocessor by using only standard digital ports.

The proposed readout system is shown in Fig. 13. The system operates with a ± 5 V supply voltage, which generally does not require additional special protection or level shifters blocks, except in one case (see the block using bipolar transistor). The readout demonstration targets sensing applications that process or generate very slowly varying physical quantities. The sensed (input) waveforms are generated by an RC divider, acting as the DUT or the source of the sensed quantity, excited by a 1 Hz sine wave with an amplitude of 1 V. Due to the large time constant (100 ms) of the DUT, a visible phase shift occurs between the excitation wave $v_{test}(t)$ and the sensed wave $v_{out}(t)$. Two single-threshold comparators are used to indicate zero-crossing moments in both waveforms, generating bipolar rectangular signals $v_{comp1,2}(t)$. Then, the rectangular bipolar signal is processed by proposed differentiator in order to create very narrow peaks (i.e. corresponding with the time constant settings $\tau_{diff} \ll t_{per}$). These signals are processed by the proposed differentiator, using the first topology from Fig. 2. It allows precise tuning to shape the square wave edges into sharp peak impulse at each rising and falling edge, denoted as $v_{p1,2}(t)$. Since the differentiator has an inverting configuration, the polarity of output peaks is inverted relative to the input edges. A diode limiter (selecting only the negative peaks $v_{p1n,2n}(t)$) is used to extract time markers corresponding to the zero-crossing moments of the sensed waveforms in the rising direction. The system then requires polarity inversion from negative to positive peaks, which is achieved by a block of analog inverters generating $v_{SET}(t)$, $v_{RESET}(t)$. The resulting positive peaks can be easily processed by a digital RS flip-flop, which directly generates a pulse signal $v_{pw}(t)$ with a width t_{pw} equal to the time difference between the zero-crossing moments of the sensed sine waveforms. The last single block generates an impulse with a duration of proportional to the signal period (i.e. half the period). This information is derived from the $v_{test}(t)$ wave using the first zero-crossing comparator. The output of the comparator is connected to a simple bipolar transistor switch whose base input is protected by a parallel diode to handle negative polarity voltages. The phase shift difference is then calculated as $\Delta\varphi = t_{pw}/t_{per} \cdot 360°$, where t_{per} is the period of the waveform. The microprocessor can easily determine the phase shift by measuring the duration of digital pulses. In this case, the phase shift generated by the DUT's RC two-port at a frequency of 1 Hz is $\Delta\varphi = 35.1°$.

The impact of the supply voltage on the application (specifically, the readout) is mainly observed in the amplitude level of the generated pulse that represents the duration of a complete period. This effect arises from the simplified circuit solution of this subpart, which is based on a basic bipolar switch. However, the variation in pulse amplitude can be reduced using a diode limiter, for example. Importantly, the time difference that defines the phase shift between the two signals (the output of the RS flip-flop) remains unaffected. Although the amplitude of the impulse may vary, it does not significantly interfere with the correct identification of the minimal TTL high (H) level. As a result, the impact is considered negligible, since the pulse width (duration) is the critical parameter being processed, not the amplitude levels. To ensure reliable operation, the supply voltage should not drop below ± 4 V.

Fig. 14 captures the entire operation in detail, based on a PSpice simulation of the system shown in Fig. 13. The simulation-based results show a pulse width of t_{pw} = 97 ms and a half-period $t_{per}/2$ = 500 ms.

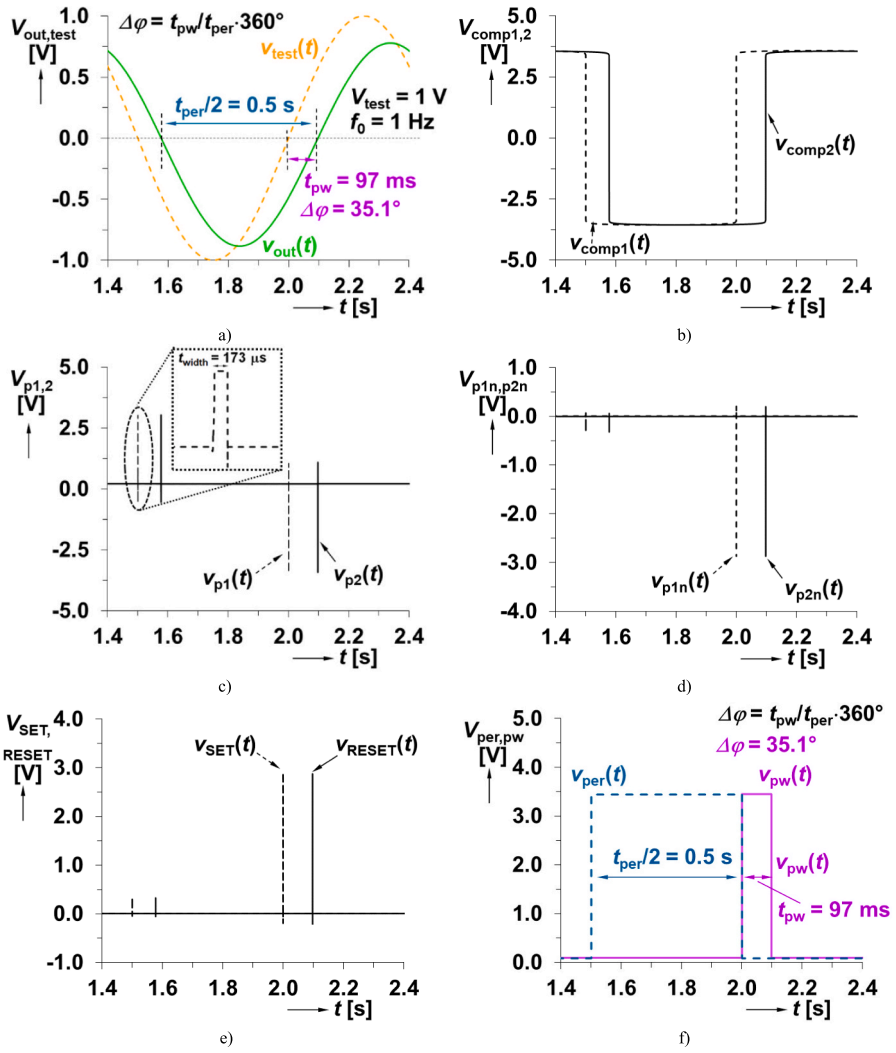

Fig. 14. Waveforms observed in the developed phase-shift difference measuring readout: a) sensed signals, b) outputs of the comparator bank, c) outputs of the differentiators, d) output of the positive limiters, e) outputs of the analog inverters, f) outputs of the RS flip flop and bipolar switch.

Table A1
Selected features of the used VGA devices (±5 V supply).

Parameter	VCA810 [37]	VCA824 [38]	AD835 [44]
Resistance of voltage inputs	1 MΩ	1 MΩ	100 kΩ
Resistance of current auxiliary inputs	–	units-tens of Ω	–
Resistance of voltage auxiliary inputs	–	> 100 kΩ	60 kΩ
Output resistance	200 mΩ	< 10 mΩ	1 Ω
Maximal output current	± 40 mA	± 50 mA	± 70 mA
Slew rate	300 V/µs	1700 V/µs	1000 V/µs
Bandwidth	30 MHz	170 MHz	150 MHz
The worst voltage linear range of transfer	≤ ±1.2 V	≤ ±1.5 V	≤ ±1.2 V
The worst current linear range of transfer	–	≤ ±2 mA	–
Gain control (A)	exponential $10^{2(\lvert V_{ser\_A}\rvert-1)}$	linear $(V_{set\_B}+1)\cdot R_f/R_g$	linear $V_{set\_A}\cdot(1+R_{f1}/R_{f2})$

Using the previously presented formula, the calculated phase shift is nearly identical to the expected theoretical value, with a difference only in the second decimal place. All simulation parameters and circuit details are shown in Fig. 13.

Table A2
Selected features of the used opamp devices (±5 V supply).

Parameter	LT1364 [35]	OPA2652 [36]
Resistance of voltage inputs	5 MΩ	35 kΩ
Output resistance	0.7 Ω	60 mΩ
Maximal output current	± 30 mA	± 100 mA
DC gain	65 dB	63 dB
Slew rate	1000 V/µs	330 V/µs
Bandwidth	> 50 MHz	700 MHz
The worst voltage linear range of transfer	≤ ±3.3 V	≤ ±3.0 V

4. Conclusion

The improvements in active building blocks for analog signal processing are very popular and useful topics of current research, see for example [49,50]. This paper introduced two novel solutions for scalable and electronically adjustable differentiators, utilizing a special VGAs and an opamp. The proposed approaches extend the time constant of a standard single opamp differentiator through resistor ratio scaling while also introducing electronic adjustability to these designs. A key advantage of these differentiators is their high and frequency-independent input impedance, in contrast to traditional single opamp-based solutions, where the input is connected directly to a capacitor terminal. Among the two implementations, the VCA824-based solution offers the

widest range of time constant adjustment given by its unique gain control mechanism. Specifically, its driving voltage can take both positive and negative values (range: −0.95 V to 1 V), whereas the AD835-based solution operates within a more limited range (0.05 V to 1 V). However, in both cases, the time constant varies linearly with the applied DC driving voltage. The selected time constant values differ intentionally between the proposed solutions, but their time constant ratios $\tau_{diff\_max}/\tau_{diff\_min}$ are comparable. The VCA824-based differentiator achieves a ratio of 70, while the AD835-based design reaches 20. The operational frequency range extends from a few kHz to several tens of kHz. In addition, the most significant parasitic effects were analyzed, including limitations introduced by the finite input impedance of the VGA and resonant peaks that could lead to instability issues. The primary source of variation in the differentiator shown in Fig. 2 is temperature, with deviations of up to ± 15 %. A comprehensive performance comparison of the two proposed solutions is presented in Table 1.

These research results are important in various areas of the electrical engineering applications for sensing purposes (readout systems) [51,52]. Application examples demonstrating waveform shaping and basic differentiator operation – such as the derivative of a sine wave, peak generation at the edge of a rectangular wave, and constant detection based on a linearly rising slope – are presented in Fig. 9 to confirm the functional validity of the proposed concept. To demonstrate its practical usability, the VCA824-based differentiator was implemented in an application example that demonstrates a sensor readout system for absolute phase shift difference measurement. The approach relies on simple analog processing to encode phase shift information into the pulse width of the generated impulses, allowing for digital processing without the need for an ADC. The validity of the proposed designs was confirmed by detailed PSpice simulations. In the application example, the most notable influence comes from variations in the supply voltage. This is because the period-defining impulse is generated by a simple bipolar switch. However, this variation affects only the amplitude of the impulse, not the accuracy of the time interval detection. The amplitude variation can be effectively mitigated by using limiters.

Future work will focus on implementing these differentiators in similar systems as discussed in **Section 3.3** allowing specific adjustable signal operations, event detection, and general sensing readout design. The electronic adjustability of the differentiators provides key advantages for automation and in-field adaptability.

CRediT authorship contribution statement

Roman Sotner: Writing – review & editing, Writing – original draft, Visualization, Validation, Supervision, Methodology, Investigation, Formal analysis, Data curation, Conceptualization. **Ladislav Polak:** Writing – review & editing, Visualization, Validation, Supervision, Formal analysis. **Jiri Petrzela:** Writing – review & editing, Visualization, Validation, Data curation, Conceptualization. **Dmitrii Semenov:** Writing – review & editing, Visualization, Validation. **Lukas Langhammer:** Writing – review & editing, Visualization, Validation, Supervision. **Winai Jaikla:** Writing – review & editing, Visualization, Validation, Supervision.

Declaration of competing interest

The authors declare that they have no known competing financial interests or personal relationships that could have appeared to influence the work reported in this paper.

Acknowledgement

This work was supported by the institutional support of the Ministry of Defence of the Czech Republic.

Appendix A. – Parameters of used active devices

Appendix B. – Principle of VCA824 (MCDU-VGCA-CFOA)

This device has three high-impedance inputs, marked as Y_1, Y_2, Y_C, three low-impedance current inputs, marked as X_1, X_2, F, a single low-impedance voltage output labeled as O and a single voltage gain-driving input (designated as V_{set_B}). Internally, the device contains two second-generation current conveyors (CCIIs) [39–41], hence: $V_{Y1} = V_{X1}$, $V_{Y2} = V_{X2}$ ($I_{Y1} = I_{Y2} = 0$). The currents I_{X1} and I_{X2} are copied to the I_{Z1} and I_{Z2} outputs of the internal CCIIs, respectively. The difference between these currents is I_i, which is amplified by the VGCA according to $I_o = (I_{X1} - I_{X2})\cdot B$. The auxiliary terminal F allows for additional current injection, contributing to the output current as I_o ($I_x = I_o + I_F$). Meanwhile, the CFOA ensures the voltage condition $V_{Yc} = V_F$ (with $I_{Yc} = 0$). The output of the CFOA, serving as the output of the device, accurately reproduces the voltage from an internal high-impedance node. The current gain of the VGCA device can be electronically adjusted according to $B \cong 1/2\cdot(V_{set\_B} + 1)$. This gain can be varied between 0 and 1 by adjusting V_{SET_B} in the range of –1 V to 1 V.

References

[1] P. R. Gray, P. J. Hurst, S. H. Lewis and R. G. Meyer, Analysis and design of analog integrated circuits (5th ed.). USA: Wiley, 2009. ISBN 978-0471321682.
[2] Sotner R, Polak L, Jerabek J, Petrzela J, Kledrowetz V. Analog Multipliers-Based Double Output Voltage Phase Detector for Low-Frequency Demodulation of Frequency Modulated Signals. IEEE Access 2021;9:93062–78. https://doi.org/10.1109/ACCESS.2021.3092525.
[3] Sotner R, Jerabek J, Polak L, Prokop R, Kledrowetz V, Theumer R, et al. Special analog multipliers in voltage-controlled oscillator and phase-locked loop-based FM demodulator for measurement and processing of sensed low-frequency signals. Measurement 2022;201:1–17. https://doi.org/10.1016/j.measurement.2022.111734.e.
[4] Al-Absi MA, Al-Khulaifi AA. A New Floating and Tunable Capacitance Multiplier with Large Multiplication Factor. IEEE Access 2019;7:120076–81. https://doi.org/10.1109/ACCESS.2019.2936800.
[5] Al-Absi MA, M. T. Abuelma'atti. A Novel Tunable Grounded Positive and Negative Impedance Multiplier. Ieee transactions on Circuits and Systems II: Express Briefs 2019;66(6):924–7. https://doi.org/10.1109/TCSII.2018.2874511.
[6] D. Biolek, J. Vavra and. A. Ü. Keskin, "CDTA-Based Capacitance Multipliers," Circuits Syst Signal Process, vol. 38, pp. 1466–1481, 2019. doi: 10.1007/s00034-018-0929-y.
[7] Sotner R, Jerabek J, Polak L, Petrzela J. Capacitance Multiplier Using Small Values of Multiplication Factors for Adjustability Extension and Parasitic Resistance Cancellation Technique. IEEE Access 2020;8:144382–92. https://doi.org/10.1109/ACCESS.2020.3014388.
[8] Al-Absi MA, Al-Khulaifi A. A Novel Tunable Grounded Positive and Negative Active Inductor Simulator and Impedance Multiplier. Arab J Sci Eng 2022;47:14983–8. https://doi.org/10.1007/s13369-022-07338-8.
[9] Al-Absi MA. A novel compact and tunable positive and negative impedance simulator and multiplier. Int J Circuit Theory Appl 2023;52(3):1587–96. https://doi.org/10.1002/cta.3832.
[10] M. Vahbeh, E. Özer, and F. Kaçar, "Design of Lossless Negative Capacitance Multiplier Employing a Single Active Element," Electronics, vol. 13, no. 6, pp. 1–20, doi: 10.3390/electronics13061163.
[11] Özer E. Electronically Tunable CFTA Based Positive and Negative Grounded Capacitance Multipliers. AEU-Int J Electron C 2021;134:153685. https://doi.org/10.1016/j.aeue.2021.153685.
[12] Seechaiya N, et al. Electronically Tunable Grounded and Floating Capacitance Multipliers Using a Single Active Element. Journal of Electrical and Computer Engineering 2024;2024:1–17. https://doi.org/10.1155/2024/6628863.
[13] Sakac B, Özenli D. A Current Mode Capacitance Multiplier Employing a Single Active Element Based on Arbel-Goldminz Cells for Low Frequency Applications. Microelectron Eng 2024;288:112157. https://doi.org/10.1016/j.mee.2024.112157.
[14] Jeshvaghani MA, Dolatshahi M. A New Ultra-Low Power Wide Tunable Capacitance Multiplier Circuit in Subthreshold Region for Biomedical Applications. AEU-Int J Electron C 2024;177:155166. https://doi.org/10.1016/j.aeue.2024.155166.
[15] Senani R, et al. A New CMOS Grounded Positive Capacitance-Multiplier and an Up-To-Date Bibliography on Capacitance Multipliers. AEU-Int J Electron C 2025;190:155643. https://doi.org/10.1016/j.aeue.2024.155643.
[16] O'Rourke R. First and Second Order Circuits and Equations: Technical Background and Insights. Wiley-IEEE Press 2024;ISBN:978-1-119-91353-5.

[17] Kishore KL. Operational amplifiers and linear integrated circuits. Delhi: Pearson; 2008.
[18] Rincon-Mora GA. Active capacitor multiplier in Miller-compensated circuits. IEEE J Solid State Circuits 2000;35(1):26–32. https://doi.org/10.1109/4.818917.
[19] Ananda Mohan PV. Analysis of Negative-R Assisted Integrators and Differentiators. Electron Lett 2020;56(3):123–5. https://doi.org/10.1049/el.2019.2905.
[20] Alzaher H. Current Follower Based Reconfigurable Integrator/Differentiator Circuits with Passive and Active Components' Reuse. Microelectron J 2015;46(2): 135–42. https://doi.org/10.1016/j.mejo.2014.12.001.
[21] Venkateswaran P, Nandi R, Das S. New Integrators and Differentiators Using a MMCC. Circuits and Systems 2012;3(3):288–94. https://doi.org/10.4236/cs.2012.33040.
[22] Ramola V, Mishra S, Singh RK, Chauhan DS. "Design of CCCDBA Based Voltage Mode Differentiator and Integrator," in Proc. In: Of the International Conference on Advances in Electronics, Electrical and Computer Science Engineering (UACEE); 2012. p. 109–12.
[23] S.Srisoontorn et al., "Reconfigurable of Current-Mode Differentiator and Integrator Based-on Current Conveyor Transconductance Amplifiers," International Journal of Electrical and Computer Engineering (IJECE), vol. 12, no. 1, pp. 208–218, 2022, doi: 10.11591/ijece.v12i1.pp208-218.
[24] R. Sotner, J. Petrzela and L. Langhammer, :Voltage Tunable Building Blocks Using Compact Active Device in Design of Filtering Applications,: in Proc. of 31st International Conference Radioelektronika, Brno, Czech Republic, 2021, pp. 1-4, doi: 10.1109/RADIOELEKTRONIKA52220.2021.9420212.
[25] Safari L, Barile G, Stornelli V, Ferri G. An Overview on the Second Generation Voltage Conveyor: Features, Design and Applications. IEEE Trans Circuits Syst Express Briefs 2019;66(4):547–51. https://doi.org/10.1109/TCSII.2018.2868744.
[26] C. P. Singh, A. Pathania, K. Sharma, J. Madan and R. Sharma, "Design of an Integrator-Differentiator Block for a Transimpedance Amplifier using 0.18μm Technology," 2019 Devices for Integrated Circuit (DevIC), Kalyani, India, 2019, pp. 394-397, doi: 10.1109/DEVIC.2019.8783474.
[27] Lawanwisut S, Siripruchyanun M, Jaikla W. An Active-Only Temperature-Insensitive Current-Mode Biquad Filter Based on Differentiator Structures Employing CCCCTAs. Circuits and Systems 2013;4(3):280–6. https://doi.org/10.4236/cs.2013.43038.
[28] A. Jantakun, N. Pisutthipong and M. Siripruchyanun, "An active-only high output-impedance current-mode universal biquad filter and quadrature oscillator based on lossless differentiators," ECTI-CON2010: The 2010 ECTI International Confernce on Electrical Engineering/Electronics, Computer, Telecommunications and Information Technology, Chiang Mai, Thailand, 2010, pp. 32-36.
[29] Mathur K, Venkateswaran P, Nandi R. A Single Resistor Tunable Grounded Capacitor Dual-Input Differentiator. Circuits and Systems 2015;6(3):49–54. https://doi.org/10.4236/cs.2015.63005.
[30] N. Wongprommoon, P. Pienpichayapong and P. Prommee, "Tunable Elliptic High-pass Filter based on Differentiator Approach," in Proc. of the 59th Annual Conference of the Society of Instrument and Control Engineers of Japan (SICE), Chiang Mai, Thailand, 2020, pp. 382-385, doi: 10.23919/SICE48898.2020.9240232.
[31] P. Prommee, N. Wongprommoon, F. Khateb and N. Manositthichai, "Simple Structure OTA-C Elliptic Band-pass Filter," in Proc. of the 16th International Conference on Electrical Engineering/Electronics, Computer, Telecommunications and Information Technology (ECTI-CON), Pattaya, Thailand, 2019, pp. 729-732, doi: 10.1109/ECTI-CON47248.2019.8955258.
[32] Bhargav A, Saini JK. A Novel Simple Differentiator Circuit Based on Carbon Nano Tube Field Effect Transistors Voltage Difference Transconductance Amplifier. Micro and Nanosystems 2019;11(2):133–41. https://doi.org/10.2174/1876402911666190527085225.
[33] N. Chomnak and N. Wongprommoon, "MO-CCCII High-Order Chebyshev Notch Filter," in Proc. of the 21st International Conference on Electrical Engineering/Electronics, Computer, Telecommunications and Information Technology (ECTI-CON), Khon Kaen, Thailand, 2024, pp. 1-4, doi: 10.1109/ECTI-CON60892.2024.10594911.
[34] Pandey N, Pandey R, Anurag R, Vijay R. A class of differentiator based multifunction biquad filters using OTRAs. Advances in Electrical and Electronic Engineering 2020;18(1):31–40. https://doi.org/10.15598/aeee.v18i1.3363.
[35] LT1364/LT1365: Dual and Quad 70MHz, 1000V/μs Op Amps, Datasheet, 12 pages, Accessed on 2025. 2. 8.: https://www.analog.com/media/en/technical-documentation/data-sheets/13645fa.pdf.
[36] OPA2652Dual, 700MHz, Voltage-Feedback Operational Amplifier, Datasheet, 24 pages, Accessed on 2025. 2. 8.: https://www.ti.com/lit/ds/symlink/opa2652.pdf.
[37] VCA810: High Gain Adjust Range, Wideband and Variable Gain Amplifier, Datasheet, 42 pages, Accessed on 2025. 2. 8.: https://www.ti.com/lit/ds/symlink/vca810.pdf.
[38] VCA824 Ultra-Wideband, > 40-dB Gain Adjust Range, Linear in V/V Variable Gain Amplifier, Datasheet, 44 pages, Accessed on 2025. 2. 8.: https://www.ti.com/lit/ds/symlink/vca824.pdf.
[39] Biolek D, Senani R, Biolkova V, Kolka Z. Active elements for analog signal processing: Classification, Review and New Proposals. Radioengineering 2008;17(4):15–32.
[40] H. Kuntman and D. Özenli, „Current Conveyors, Variants, and Applications," Trends in Circuit Design for Analog Signal Processing. Analog Circuits and Signal Processing. Springer, Cham, 2022, doi: 10.1007/978-3-030-96836-6_3.
[41] Senani R, Bhaskar DR, Singh VK, Sharma RK. Current Conveyors: Variants, Applications and Hardware Implementations. Switzerland: Springer International Publishing; 2015.
[42] Sotner R, et al. Modified Current Differencing Unit and its Application for Electronically Reconfigurable Simple First-order Transfer Function. Advances in Electrical and Computer Engineering 2015;15(1):3–10.
[43] Sotner R, Jerabek J, Polak L, Jaikla W, Andriukaitis D. Compact active analog device for novel applications useful for sensing and measurement. Measurement 2024;235:1–11. https://doi.org/10.1016/j.measurement.2024.114896.
[44] AD835, 250 MHz, Voltage Output, 4-Quadrant Multiplier, Datasheet, 14 pages, Accessed on 2025. 2. 8.: https://www.analog.com/media/en/technical-documentation/data-sheets/ad835.pdf.
[45] Sharma D, Nath V. CMOS Operational Amplifier Design for Industrial and Biopotential Applications: Comprehensive Review and Circuit Implementation. Results Eng 2024;22:102357. https://doi.org/10.1016/j.rineng.2024.102357.
[46] Häberle M, Djekic D, Fantner GE, Lips K, Ortmanns M, Anders J, et al. IEEE 44th European Solid State Circuits Conference (ESSCIRC). Dresden, Germany 2018; 2018:294–7. https://doi.org/10.1109/ESSCIRC.2018.8494290.
[47] Tseng C-H, Yu L-T, Huang J-K, Chang C-L. A Wearable Self-Injection-Locked Sensor with Active Integrated Antenna and Differentiator-Based Envelope Detector for Vital-Sign Detection from Chest Wall and Wrist. IEEE Trans Microw Theory Tech 2018;66(5):2511–21. https://doi.org/10.1109/TMTT.2017.2785793.
[48] Simmich S, Bahr A, Rieger R. Noise Efficient Integrated Amplifier Designs for Biomedical Applications. Electronics 2021;10(13):1–17. https://doi.org/10.3390/electronics10131522.
[49] Yosefi G. A special technique for Recycling Folded Cascode OTA to improve DC gain, bandwidth, CMRR and PSRR in 90 nm CMOS process. Ain Shams Eng J Jun. 2020;11(2):329–42. https://doi.org/10.1016/j.asej.2019.08.018.
[50] Sharroush SM, Abdalla YS. Two proposed BiCMOS inverters with enhanced performance. Ain Shams Eng J Apr. 2023;15(1):102259. https://doi.org/10.1016/j.asej.2023.102259.
[51] Hertz PY, et al. CMOS readout FEE based TV-BLR module for CdZnTe pixel detectors in high count rate applications. Ain Shams Eng J May 2023;15(1): 102303. https://doi.org/10.1016/j.asej.2023.102303.
[52] A. Ali et al., "Sensorless microcontroller-based zero-crossing detection system for AC signals using a rounding function," Ain Shams Engineering Journal, p. 102375, Jul. 2023, doi: https://doi.org/10.1016/j.asej.2023.102375.

Roman Sotner (S'08–M'12) was born in Znojmo, Czech Republic, in 1983. He received the Ph.D. and M.Sc. degrees in Electrical Engineering from the Brno University of Technology, Czech Republic, in 2012 and 2008, respectively. Currently, he is an Associate Professor at the Department of Radio Electronics, Faculty of Electrical Engineering and Communication, Brno University of Technology, Brno, Czech Republic. His interests are discrete as well as integrated analog circuits (active filters, oscillators, audio, etc.), circuits in the current mode, circuits with direct electronic controlling possibilities, especially analog signal processing in sensing applications and computer simulation. He is a member of IEEE.

Ladislav Polak was born in Štúrovo, Slovakia in 1984. He received the M.Sc. degree in 2009 and the Ph.D. degree in 2013, both in Electronics and Communication from the Brno University of Technology (BUT), Czech Republic. He is currently an Associate Professor at the Department of Radio Electronics (DREL), BUT. His research interests are wireless communication systems, RF measurements, signal processing and computer-aided analysis. He is a member of IEEE.

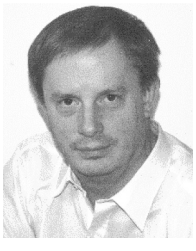

Jiri Petrzela was born in Brno, Czech Republic, in 1978. He received M.Sc. and Ph.D. degree in field of theoretical electronics, in 2003 and 2007 respectively. Currently, he is working as Associate Professor at Department of Radio Electronics, Faculty of Electrical Engineering and Communications, Brno University of Technology, Czech Republic. His research interest covers numerical methods in electrical engineering, nonlinear dynamics, chaos theory, analog lumped circuit design and computer-aided analysis. He is a main author or co-author of more than 30 journal papers and 40 international conference contributions.

Dmitrii Semenov is an undergraduate senior student at the Department of Radio Electronics, Faculty of Electrical Engineering and Communication, Brno University of Technology, Brno, Czech Republic. He also works as an Analog Design Intern at semiconductor supplier "onsemi". His interests are integrated analog circuits (active filters, operational amplifiers, references, etc.), analog signal processing, circuit design based on operational transconductance amplifiers (OTA), and global optimization methods.

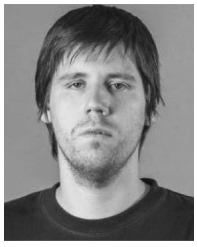

Lukas Langhammer received the M.Sc. and Ph.D. degrees in electrical engineering and telecommunication from the Faculty of Electrical Engineering and Communication, Brno University of Technology (BUT), Brno, Czech Republic, in 2012 and 2016, respectively. He is currently working with the Department of Electrical Engineering, Faculty of Military Technology, University of Defence, Brno, and also with the Department of Telecommunications, Faculty of Electrical Engineering and Communication, BUT. His research interests include design and analysis of frequency filters, basic analog building blocks, and advanced active elements.

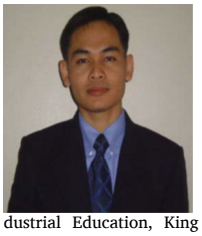

Winai Jaikla was born in Buriram, Thailand. He received the B. S.I.Ed. degree in Telecommunication Engi-neering from the King Mongkut's Institute of Technology Ladkrabang (KMITL), Thailand in 2002, M.Tech.Ed. in Electrical Technology and Ph. D. in Electrical Education from King Mongkut's University of Technology North Bangkok (KMUTNB) in 2004 and 2010, respectively. From 2004 to 2011 he was with Electric and Electronic Program, Faculty of Industrial Technology, Suan Sunandha Rajabhat University, Bangkok, Thailand. He has been with the Department of Engineering Education, Faculty of Industrial Education, King Mongkut's Institute of Technology Ladkrabang, Bangkok, Thailand since 2012. His research interests include electronic communication, analog signal processing and analog integrated circuits. He is a member of ECTI, Thailand.